energy&fuels

Article

pubs.acs.org/EF

Experimental and Theoretical Study on the Pyrolysis Mechanism of Three Coal-Based Model Compounds

Gang Li,[†,‡] Lu Li,[†,‡] Lei Shi,[‡] Lijun Jin,[†] Zichao Tang,*[,‡] Hongjun Fan,*[,‡] and Haoquan Hu*[,†]

[†]State Key Laboratory of Fine Chemicals, Institute of Coal Chemical Engineering, School of Chemical Engineering, Dalian University of Technology, Dalian 116024, People's Republic of China

[‡]State Key Laboratory of Molecular Reaction Dynamics, Dalian Institute of Chemical Physics, Chinese Academy of Sciences, Dalian 116023, People's Republic of China

ABSTRACT: An experimental study of three coal-based model compound (anisole, phenyl ethyl ether, and *p*-methyl anisole) pyrolysis was carried out at low pressure (below 50 Pa) within the temperature range from 573 to 1323 K. The pyrolysis process was investigated by detecting the reactants, radicals, and products using vacuum ultraviolet single-photon ionization time-of-flight mass spectrometry. The similarities and differences of three model compounds in the pyrolysis process were discussed. The results suggested that the radical reactions were dominant in the pyrolysis process at higher temperatures, whereas the intermolecular reactions were significant at lower temperatures. β−H was a key factor for the non-radical reactions. The PhO−C homolytic bond scission was the first step for the radical reaction. Substituents on the benzene ring play an important role in the pyrolysis process of phenyl ethers, which can directly form conjugated stable structure compounds. These observations were supported by our theoretical calculation at the mPW2PLYP level.

1. INTRODUCTION

Pyrolysis is one of the most important coal processes because it occurs in most coal conversion processes, such as combustion, gasification, carbonization, liquefaction, etc.; it is also an attractive technology for effective utilization of coal, which can be used for upgrading low-rank coal and obtaining a liquid product before combustion or other use. Therefore, understanding the pyrolysis behavior is important to develop new coal utilization technologies and provide information about the physicochemical structure of coal.[1−5] As is known, the organic portion of coal predominantly consists of polycyclic aromatic, hydroaromatic, and heterocyclic clusters joined together into a cross-linked three-dimensional network by short aliphatic and ether linkages. The aromatic rings are substituted with alkyl side chains and phenolic hydroxyl and ether groups.[6] All of these coal processes are directly associated with homolytic bond dissociations of the organic structures of coal into smaller fragments. The studies on the thermochemical mechanisms are very important for practical manipulating process conditions. However, the thermochemical mechanistic understanding of these reactions at a molecular level is very difficult because of the complexity, heterogeneity, and variability of coal. For these reasons, the thermolysis of the coal-based model compounds for individual structural features in coal was performed and proved to be a useful research method.

Generally, phenyl ethers often serve as the model compounds for the low-rank coal and lignin from biomass.[7−9] The pyrolysis behaviors of anisole (m/z 108) as the most simple phenyl ether has been studied in detail.[10−16] Arends et al.[10] studied the kinetics behavior of the formation of the phenoxy radical in anisole pyrolysis and determined the pre-exponential factor (2×10^{15} s^{-1}) of this reaction and the activation energy (64 kcal/mol). Many groups investigated the kinetics of the primary pathway for the phenoxyl radical to generate the cyclopentadienyl radical and generally agreed with the pre-exponential factor (7.40×10^{11} s^{-1}) and activation energy (43.86 kcal/mol).[17−19] However, this reaction is not a simple bond scission, and the reactivation energy cannot conform very well. The cyclopentadienyl radical is considered as an important intermediate for the formation of polycyclic aromatic hydrocarbons in combustion processes.[20−22] Because of its stability, the cyclopentadienyl radical can keep a high concentration during combustion or pyrolysis processes. It can react with other species to form polycyclic aromatic hydrocarbons. For example, methylcyclopentadiene can be generated by combining the cyclopentadienyl radical with the methyl radical and further forms benzene through the dehydrocyclization. Besides, two cyclopentadienyl radicals can recombine to produce naphthalene through allyl cyclopropyl intermediates.[22] Some aspects of anisole pyrolysis have been studied previously and reveal the common pyrolysis characteristics of phenyl ethers. However, with the change of the substituent, the pyrolysis behaviors of phenyl ethers will be different. The study about the influence of the substituent on the pyrolysis of phenyl ethers is scarce.

In this work, anisole, phenyl ethyl ether, and *p*-methyl anisole were selected as the model compounds based on the following considerations: Anisole is served as the most simple phenyl ether, and its pyrolysis behavior generally reveals the common pyrolysis characteristics of phenyl ethers. Phenyl ethyl ether was chosen to examine the effect of β−H on the phenyl ether pyrolysis. To obtain more information about the pyrolysis of phenyl ethers, we also studied the influence of the alkyl substituent on the benzene ring via understanding the pyrolysis

Received: November 18, 2013
Revised: January 9, 2014
Published: January 9, 2014

   dx.doi.org/10.1021/ef402273t | *Energy Fuels* 2014, 28, 980−986

properties of *p*-methyl anisole. Single-photon ionization time-of-flight mass spectrometry (SPI−TOF−MS) coupled with molecular-beam sampling was employed to detect the pyrolysis products. The high mass resolution and soft-ionized vacuum ultraviolet (VUV) light can help identify most species and reduce fragmentation via near-threshold photoionization, which enables the unambiguous detection of intermediates. On the basis of the experimental and theoretical analyses, the similarities and differences of the pyrolysis behaviors of three model compounds were summarized and the general pyrolysis characteristics of phenyl ethers were obtained.

2. EXPERIMENTAL SECTION

2.1. Experimental Method. A detailed description of the pyrolysis apparatus with a molecular-beam sampling mass spectrometer was reported elsewhere.[23,24] The experimental apparatus mainly includes three parts: a pyrolysis chamber with a flow reactor electronically heated by a tungsten heater, a differentially pumped chamber with a molecular-beam sampling system, and a photoionization chamber with a homemade reflection time-of-flight mass spectrometer (RTOF−MS). A cone-like nozzle with a 0.5 mm orifice is used to sample the pyrolysis species, including the reactants, intermediates, and products. The molecular beams of the pyrolysis species produced in the differential pumped chamber enter into the photoionization chamber through a skimmer. The molecular beam is ionized by a 10.6 eV VUV lamp (PKS106, Heraeus, Ltd., Germany) in the ionization region. Then, ions produced by the VUV light are drawn out of the photoionization region by a pulse extraction field triggered with a pulse generator (DG535, SRS) and detected by a microchannel plate (MCP) detector. The ion signal is recorded by a multiscaler (P7888, FAST Comtec) after being amplified with a preamplifier (SR445A, SRS).

The mixture of reactants and Ar as carrier gas passes into an alumina tube (2 mm inner diameter and 250 mm length), and a 50 mm length is heated by a tungsten heater. Ar is controlled by a mass flow controller with the flow rate of 100 standard cubic centimeters per minute (SCCM). The reactant steam was produced by bubbling high-purity Ar through reactant liquid in a container at room temperature, and the flow rates of anisole, phenyl ethyl ether, and *p*-methyl anisole are 0.017, 0.016, and 0.006 SCCM, respectively. To reduce collisions of the pyrolysis species and detect the intermediates, including radicals, the pressure of the pyrolysis chamber was kept in the range of 10−50 Pa in this work. The temperature of the flow tube was measured by a *K*-type thermocouple (Φ = 1 mm). Anisole (99%) was purchased from J&K Scientific Co., Ltd. (Beijing, China), and phenyl ethyl ether (99%) and *p*-methyl anisole (99%) were purchased from Acros Organics Co., Ltd. (Morris Plains, NJ). All chemicals were used without further purification.

A semi-quantitative analysis method was used to estimate the relative concentration, which has been reported in detail.[25] Briefly, for species *i*, the ion signal intensity I_i in the mass spectrum can be expressed by the following equation:

$$I_i = C\rho_i\sigma_i(E)$$

where C is a constant for the instrument, ρ_i is the concentration of species *i*, and $\sigma_i(E)$ is the photoionization cross-section of species *i* at the photon energy E. The relative concentration x_i of species *i* can be expressed as

$$x_i = \frac{\frac{I_i}{\sigma_i(E)}}{\sum_i \frac{I_i}{\sigma_i(E)}}$$

In our experiment, most of the species in pyrolysis can be ionized at 10.6 eV photon energy. The average photoionization cross-sections $\sigma_i(E)$ at 10.6 eV were estimated in the literature[24,26,27] and available in the online database.[28]

2.2. Computational Method. All calculations were carried out with the Gaussian 09 program.[29] A new double hybrid functional mPW2PLYP has been chose to balance accurate results with computational economy to the greatest extent.[30] The mPW2PLYP/cc-pVDZ[30,31] was used for all geometry optimizations and vibrational frequency calculations. Single-point energies were calculated at the mPW2PLYP/cc-pVTZ[32] level at the optimized geometries. The thermodynamic corrections were obtained using harmonic oscillator approximation and unscaled vibrational frequencies.

The enthalpy $H(T)$ was calculated using the following equation:[33]

$$H(T) = E + \mathrm{ZPE} + H_{\mathrm{trans}} + H_{\mathrm{rot}} + H_{\mathrm{vib}} + RT$$

where E is the electronic energy, ZPE is the zero-point energy, H_{trans}, H_{rot}, and H_{vib} are the translational enthalpy, rotational enthalpy, and vibrational enthalpy, respectively, R is the universal gas constant, and T is the temperature. All relative enthalpies correspond to 298 K values in kcal/mol.

3. RESULTS AND DISCUSSION

3.1. Similarity in the Pyrolysis Process of Three Phenyl Ethers. In this work, the results are primarily concluded from the measurements of photoionization mass spectra. Figures 1−3 show a series of partial mass spectra taken at

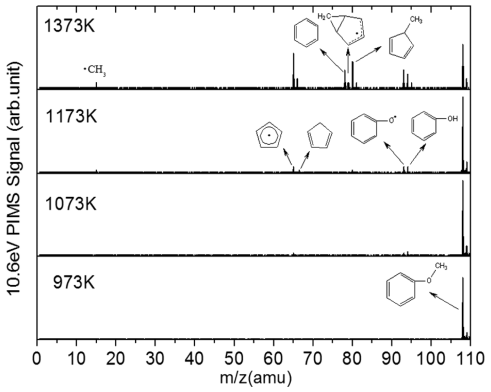

Figure 1. Photoionization mass spectra of anisole taken with selected temperatures at a photoenergy of 10.6 eV.

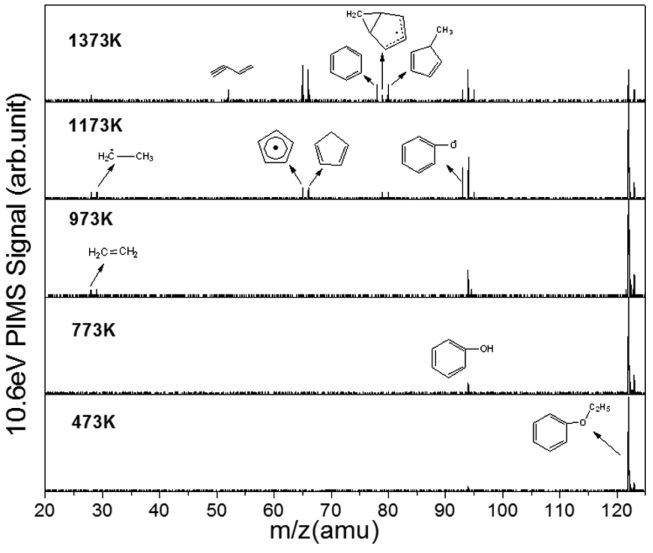

Figure 2. Mass spectra of the pyrolysis products from phenyl ethyl ether at selected temperatures at a photoenergy of 10.6 eV.

dx.doi.org/10.1021/ef402273t | *Energy Fuels* 2014, 28, 980−986

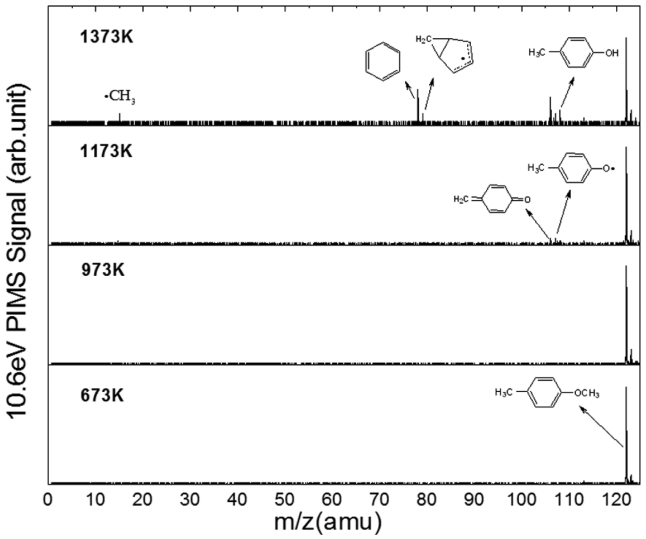

Figure 3. Photoionization mass spectra of *p*-methyl anisole taken with selected temperatures at a photoenergy of 10.6 eV.

10.6 eV and different temperatures labeled on the figures. These mass spectra illustrated in Figures 4–6 were used to evaluate

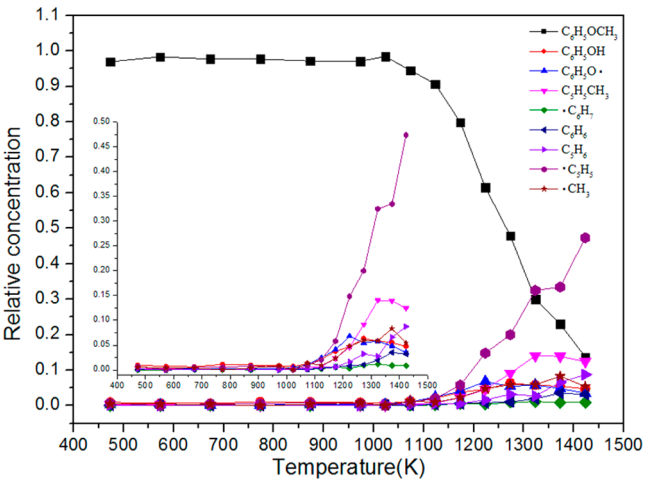

Figure 4. Plots of the relative concentration of the peaks in the mass spectra from pyrolysis of anisole as a function of the temperature. To present plots clearly, species ion relative concentrations are amplified.

the relative concentration plots. As seen from Figures 4–6, the pyrolysis process of anisole, phenyl ethyl ether, and *p*-methyl anisole are similar, because of their analogous structure. The parent ions are prominent in the mass spectrum at the lower temperature and begin to decompose, and the relative concentration of species increases when the pyrolysis furnace is heated to around 1000 K.

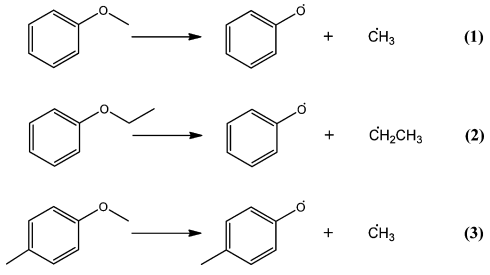

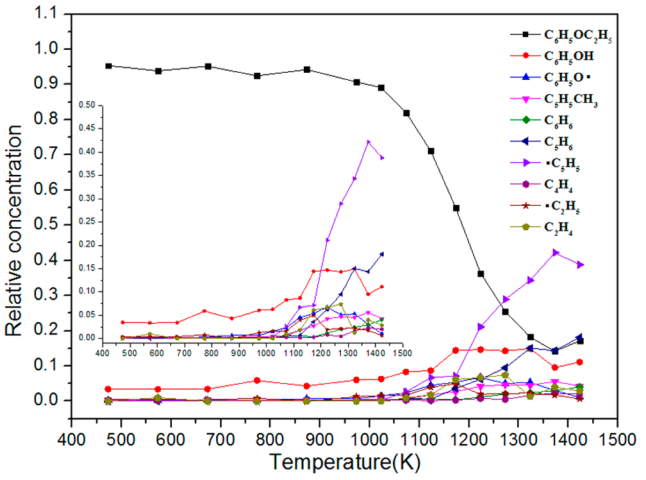

Figure 5. Plots of the relative concentration of the peaks in the mass spectra from pyrolysis of phenyl ethyl ether as a function of the temperature. To present plots clearly, species ion relative concentrations are amplified.

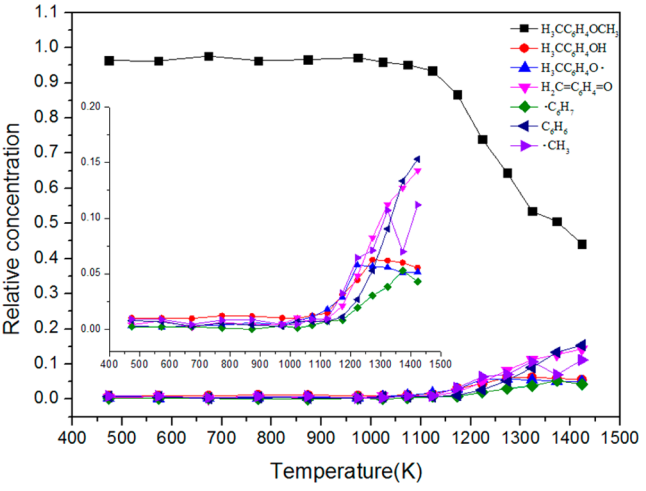

Figure 6. Plots of the relative concentration of the peaks in the mass spectra from pyrolysis of *p*-methyl anisole as a function of the temperature. To present plots clearly, species ion relative concentrations are amplified.

All of those fragments first come from PhO–C bond scission shown in reactions 1–3. The initial formation temperature of the phenoxy radical (*m*/*z* 93) and *p*-methyl phenoxy radical (*m*/*z* 107) is around 1000 K, and their relative concentrations reach the peak at 1223 K. We have calculated bond dissociation enthalpies (BDEs) and compared them to the previous experimental values, as shown in Table 1. The PhO–C bond is the weakest bond in the molecule because of the resonance stabilization in the phenoxy radical and *p*-methyl phenoxy radical. As seen from Figures 1–3, the peaks at *m*/*z* 65 and 79 are observed at 1023 K, which are ascribed to the cyclopentadienyl radical and methyl cyclopentadienyl radical formed by reactions 4 and 5. Their relative concentrations increase with the temperature increasing, shown in Figures 4–6. It is noted that carbon monoxide (*m*/*z* 28) has an ionization potential of 14.01 eV, which is too high to be ionized by the VUV lamp used (10.6 eV) and is not observed here.[34] Besides, the cyclopentadienyl radical can add a hydrogen atom to generate cyclopentadiene (*m*/*z* 66).

dx.doi.org/10.1021/ef402273t | *Energy Fuels* 2014, 28, 980–986

Table 1. Experimental and Calculated Bond Dissociation Enthalpies (kcal/mol)

compounds	mPW2PLYP	experimental
$C_6H_5O-CH_3$	64.7	62 ± 3^a
$C_6H_5O-C_2H_5$	66.3	63^b
$H_3CC_6H_4O-CH_3$	62.7	
$C_6H_5-OCH_3$	99.1	101^c
$C_6H_5-OC_2H_5$	98.3	
$H_3CC_6H_4-OCH_3$	98.5	
$H_3COC_6H_4-CH_3$	101.3	

[a]From ref 46. [b]From ref 47. [c]From ref 48.

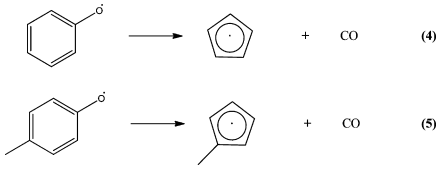

With the temperature increasing, the cyclopentadienyl radicals are decomposed into acetylene and the propargyl radical (m/z 39) (reaction 6).[35] The computational studies indicated that the barrier for this process is 62.4 kcal/mol at the G2M (rcc, MP2) level of theory, and a pressure-dependent preexponential factor of A is $2 \times 10^{68}T^{-15.0}$ s^{-1} at 1 atm.[36] However, in Figures 1−3, no signal of the propargyl radical was observed, which is possibly caused by too low of a concentration of the propargyl radical in the tubular flow reactor.

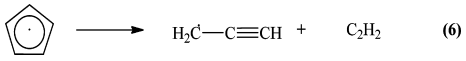

Figures 1−3 show that benzene (m/z 78) was formed in pyrolysis processes of three model compounds. All of the formation temperatures of benzene are around 1073 K, and the relative concentration of benzene increases continuously with the temperature increasing, shown in Figures 4−6. The propargyl−propargyl radical recombination mechanism, as reaction 7, is often used to explain the formation of benzene[37−39] and has been proven to be important in the combustion of acetylene and other small aliphatic molecules. However, several experimental phenomena indicated that the recombination of propargyl radicals is not the main pathway to produce benzene in our pyrolysis process of the model compounds. First, in pyrolysis processes of anisole, phenyl ethyl ether, and *p*-methyl anisole, the traces of benzene appeared at a lower temperature compared to the propargyl radical.[40] Second, the signal of the propargyl radical was not detected in the mass spectrum, suggesting that other pathways may be responsible for the majority of benzene formation.

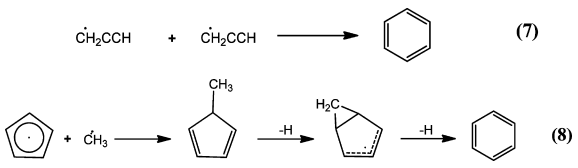

The mass peak at m/z 80 in Figures 1 and 2 is assigned to methylcyclopentadiene, an important precursor to form benzene, which is formed by the combination of the methyl radical (m/z 15) and cyclopentadienyl radical (m/z 65). Figures 4 and 5 show that the formation temperature of methylcyclopentadiene is around 1023 K. Methylcyclopentadiene can abstract two hydrogen atoms to generate benzene via a bicyclic intermediate and ring expansion (reaction 8).[41−43] The previous research to compare the pyrolysis of methylcyclopentadiene with cyclopentadiene suggested that the first trace of benzene is observed at 1173 K before any propargyl radical is detected in methylcyclopentadiene pyrolysis and no benzene was observed below 1373 K in cyclopentadiene pyrolysis.[40] In Figures 1−3, the mass peaks at m/z 79 and 78 are all clearly visible in the model compound pyrolysis at 1373 K and correspond to two subsequent hydrogen abstractions from methylcyclopentadiene, indicating that benzene is more likely to form through abstraction of two hydrogen atoms from methylcyclopentadiene rather than propargyl radical recombination. Besides, methylcyclopentadiene has three isomers (1-, 2-, and 5-methylcyclopentadiene), which all likely contribute to form benzene. The decomposition pathways of three isomers are very different and, not surprisingly, governed by very different kinetics. The thermal dissociation channels investigated by researchers[42−44] suggested that the most likely channel to form benzene for any methylcyclopentadiene isomer is via isomerization to 5-methylenecyclopentadiene, followed by ring expansion to the cyclohexadienyl radical, and then conversion of the cyclohexadienyl radical to benzene very fast. In Figure 2, vinylacetylene (m/z 52), which is from decomposition of benzene, was identified at 1373 K.[45]

3.2. Mechanism of Phenol Generated in Phenyl Ethyl Ether Pyrolysis. Phenol is the main product in tar during low-rank coal pyrolysis. In the pyrolysis processes of three model compounds, it is generated from the addition of the hydrogen atom and phenoxy radical above 1000 K. However, in Figures 2 and 5, the peak of phenol was identified below 1000 K and the growth rate of the relative concentration of phenol is relatively flat from 673 to 1023 K. To figure out the mechanism of phenol formation in the pyrolysis of phenyl ethyl ether, we have studied four possible paths that contain non-radical and radical reactions, as shown in Scheme 1 by quantum chemical calculations. In path I, 2,4-cyclohexadienone (m/z 94) is formed

Scheme 1. Possible Pathways To Generate Phenol in Pyrolysis of Phenyl Ethyl Ether

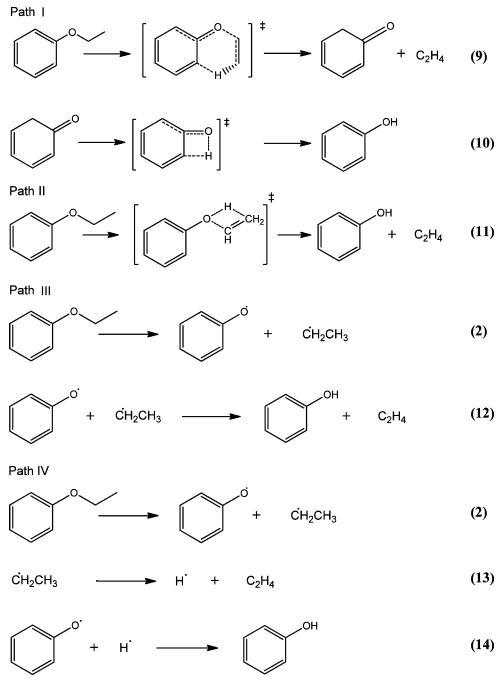

dx.doi.org/10.1021/ef402273t | Energy Fuels 2014, 28, 980−986

from the concerted reaction shown in reaction 9 and quickly converts to phenol by a 1,3 hydrogen transfer, keto−enol tautomerization, as shown in reaction 10. The rate-determining step barrier for path I has been calculated to be 55.6 kcal/mol. The second possible pathway to form the phenol is direct intermolecular hydrogen transfer, as shown in path II (reaction 11). The barrier of path II is 62.1 kcal/mol by our calculation. Paths III and IV share the same C−O homolysis (reaction 2). For this step, we can roughly take BDE as the barrier. We take C−O homolysis as the first step of paths III and IV because its BDE is the smallest in phenyl ethyl ether. The C−O homolysis barrier is calculated to be 66.3 kcal/mol. For path III, the proton transfer step (reaction 12) has a low energy barrier of 7.1 kcal/mol. For path IV, the radical recombination step is always highly exothermic with a negligible barrier. The barrier for the ethyl (m/z 29) dissociation is calculated to be 37.2 kcal/mol. On the basis of the above results and discussion, it is thought that the pathway of non-radical reactions is primarily due to their relatively low energetic cost. Notably, the values of energy above are enthalpy, and the real energy barrier of the radical reaction will decrease with the increase of the temperature because homolysis is an increasing entropy process. Therefore, we suggest that pathways of radical reactions become dominate above 1000 K, while non-radical reactions are more favorable in relatively lower temperatures.

3.3. Differences in the Pyrolysis Process of Three Phenyl Ethers. Although three model compounds have a similar decomposition pathway, their different structures make the pyrolysis processes have their own characteristics. They all produced phenol at high temperatures, but their pyrolysis behaviors at lower temperatures are quite different. As shown in the mass spectra of pyrolysis of phenyl ethyl ether (Figure 2) and the relative concentration of individual ions (Figure 5), phenol (m/z 94) gently grows and the parent ion (m/z 122) slowly decreases when the tubular reactor was heated from 673 to 1023 K, while no phenol is observed in mass spectra in the pyrolysis of anisole and *p*-methyl anisole in the low-temperature range, which is attributed to their different structures. That is, phenyl ethyl ether has β−H in its aliphatic chain, while the two others do not. Therefore, β−H is the key factor for the concerted intermolecular reaction.

A little difference in the thermal decomposition of *p*-methyl anisole and anisole exists. As shown in Figures 3 and 6, *p*-methyl anisole first loses methyl to form the *p*-methyl phenoxyl radical (m/z 107) via C−O bond dissociation, and then the *p*-methyl phenoxyl radical is inclined to isolate a hydrogen radical and simultaneously tautomerize to form 4-methylene-2,5-cyclohexadiene-1-one (m/z 106). We proposed that the reason is that 4-methylene-2,5-cyclohexadiene-1-one has a conjugate structure, which makes it stable. To verify this process, as shown in Scheme 2, the calculations were carried out and the results showed that the C−H dissociation energy of the *p*-methyl phenoxyl radical is 57.2 kcal/mol, which is lower than the energy required for C−O bond dissociation.

To investigate whether the phenoxy radical from the thermal decomposition of anisole has a similar reaction, three possible structures of the species C_6H_4O obtained by losing the hydrogen radical of the phenoxy radical were proposed in Figure 7 and calculated values were shown in Scheme 2. The results showed that the dissociation energies were 112.0, 110.8, and 110.1 kcal/mol, respectively. Obviously, this endothermic process is substantially more unfavorable compared to the *p*-methyl phenoxyl radical. It is rationalized that there is no reasonable stable structure after a hydrogen radical dissociation from the phenoxy radical, and the resulting compounds have a carbene form.

Scheme 2. Change in Energy with Respect to Hydrogen Radical Abstraction from the Corresponding Phenoxy Radicals

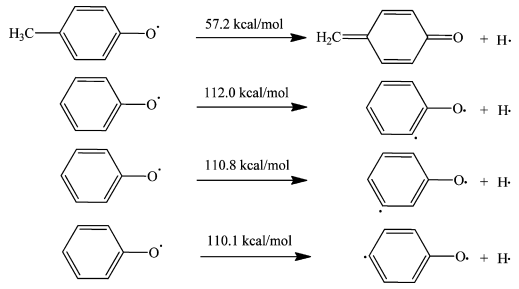

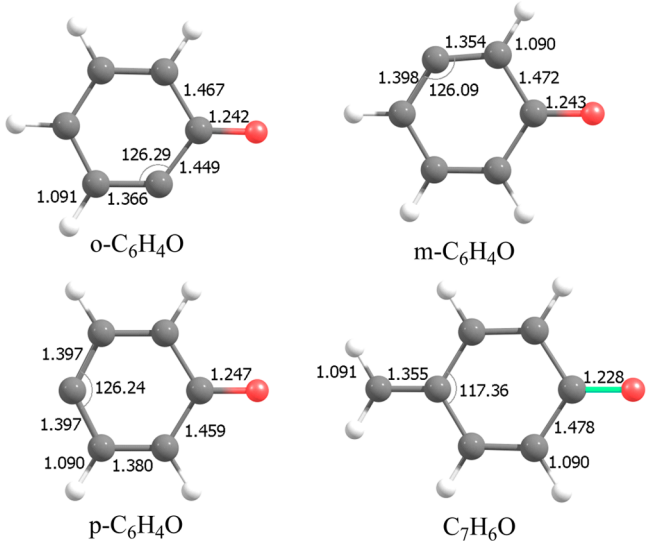

Figure 7. Molecular geometries of the resulting compounds after the phenoxy radical losing the hydrogen radical.

4. CONCLUSION

The pyrolysis behaviors of three coal-based model compounds (anisole, phenyl ethyl ether, and *p*-methyl anisole) were studied using a flow tubular reactor combined with single-photon ionization time-of-flight mass spectrometry and the semi-quantitative method. In comparison to previous studies, more pyrolysis species, especially radicals and intermediates, such as the phenoxy radical, cyclopentadienyl radical, methyl radical, etc., have been detected. The similarities of three model compounds in the pyrolysis process reveal that the radical reaction is significant at high temperatures, and the PhO−C homolytic bond scission is the first step for the radical reaction, which begins at around 1000 K. Moreover, substituents on the benzene ring play an important role in the pyrolysis process of phenyl ethers, which can straightly form a conjugate stable structure compound after a hydrogen radical dissociation from the phenoxy radical. The theoretical calculations on the formation pathways of phenol in the pyrolysis process of phenyl ethyl ether indicated that the non-radical reaction is dominant at low temperatures and β−H is a key factor for the non-radical reaction.

dx.doi.org/10.1021/ef402273t | *Energy Fuels* 2014, 28, 980−986

AUTHOR INFORMATION

Corresponding Authors

*E-mail: zctang@dicp.ac.cn.
*E-mail: fanhj@dicp.ac.cn.
*E-mail: hhu@dlut.edu.cn.

Notes

The authors declare no competing financial interest.

ACKNOWLEDGMENTS

This work was financially supported by the National Basic Research Program of China (973) (2011CB201301), the Key Program Project of the Joint Fund of Coal Research by the National Natural Science Foundation of China (NSFC) and Shenhua Group (51134014), and the Key International Science and Technology Cooperation and Exchange Projects (2013DFG60060).

REFERENCES

(1) Matsuoka, K.; Ma, Z.-x.; Akiho, H.; Zhang, Z.-g.; Tomita, A.; Fletcher, T. H.; Wójtowicz, M. A.; Niksa, S. High-pressure coal pyrolysis in a drop tube furnace. *Energy Fuels* **2003**, *17*, 984−990.

(2) Takagi, H.; Isoda, T.; Kusakabe, K.; Morooka, S. Relationship between pyrolysis reactivity and aromatic structure of coal. *Energy Fuels* **2000**, *14*, 646−653.

(3) Zhao, Y.; Hu, H.; Jin, L.; Wu, B.; Zhu, S. Pyrolysis behavior of weakly reductive coals from northwest China. *Energy Fuels* **2009**, *23*, 870−875.

(4) Zhou, Q.; Hu, H.; Liu, Q.; Zhu, S.; Zhao, R. Effect of atmosphere on evolution of sulfur-containing gases during coal pyrolysis. *Energy Fuels* **2005**, *19*, 892−897.

(5) Liu, Q.; Hu, H.; Zhou, Q.; Zhu, S.; Chen, G. Effect of inorganic matter on reactivity and kinetics of coal pyrolysis. *Fuel* **2004**, *83*, 713−718.

(6) Poutsma, M. L. Free-radical thermolysis and hydrogenolysis of model hydrocarbons relevant to processing of coal. *Energy Fuels* **1990**, *4*, 113−131.

(7) Brezny, R.; Mihalov, V.; Kovacik, V. Low-temperature thermolysis of lignins. 1. Reactions of β−O−4 model compounds. *Holzforschung* **1983**, *37*, 199−204.

(8) Brezny, R.; Surina, I.; Kosik, M. Low-temperature thermolysis of lignins. 2. Thermofractography and thermal-analysis of β−O−4 model compounds. *Holzforschung* **1984**, *38*, 19−24.

(9) Jegers, H. E.; Klein, M. T. Primary and secondary lignin pyrolysis reaction pathways. *Ind. Eng. Chem. Process Des. Dev.* **1985**, *24*, 173−183.

(10) Arends, I. W. C. E.; Louw, R.; Mulder, P. Kinetic study of the thermolysis of anisole in a hydrogen atmosphere. *J. Phys. Chem.* **1993**, *97*, 7914−7925.

(11) Suryan, M. M.; Kafafi, S. A.; Stein, S. E. The thermal decomposition of hydroxy- and methoxy-substituted anisoles. *J. Am. Chem. Soc.* **1989**, *111*, 1423−1429.

(12) Mackie, J. C.; Doolan, K. R.; Nelson, P. F. Kinetics of the thermal decomposition of methoxybenzene (anisole). *J. Phys. Chem.* **1989**, *93*, 664−670.

(13) Back, M. H. Comment on the thermal decomposition of anisole and the heat of formation of the phenoxy radical. *J. Phys. Chem.* **1989**, *93*, 6880−6881.

(14) Bruinsma, O. S. L.; Geertsma, R. S.; Bank, P.; Moulijn, J. A. Gas phase pyrolysis of coal-related aromatic compounds in a coiled tube flow reactor: 1. Benzene and derivatives. *Fuel* **1988**, *67*, 327−333.

(15) Lin, C.-Y.; Lin, M. C. Thermal decomposition of methyl phenyl ether in shock waves: The kinetics of phenoxy radical reactions. *J. Phys. Chem.* **1986**, *90*, 425−431.

(16) Pecullan, M.; Brezinsky, K.; Glassman, I. Pyrolysis and oxidation of anisole near 1000 K. *J. Phys. Chem. A* **1997**, *101*, 3305−3316.

(17) Liu, R.; Morokuma, K.; Mebel, A. M.; Lin, M. C. Ab initio study of the mechanism for the thermal decomposition of the phenoxy radical. *J. Phys. Chem.* **1996**, *100*, 9314−9322.

(18) Frank, P.; Herzler, J.; Just, T.; Wahl, C. High-temperature reactions of phenyl oxidation. *Symp. Int. Combust. Proc.* **1994**, *25*, 833−840.

(19) Baulch, D. L.; Cobos, C. J.; Cox, R. A.; Esser, C.; Frank, P.; Just, T.; Kerr, J. A.; Pilling, M. J.; Troe, J.; Walker, R. W.; Warnatz, J. Evaluated kinetic data for combustion modelling. *J. Phys. Chem. Ref. Data* **1992**, *21*, 411−734.

(20) Marinov, N. M.; Pitz, W. J.; Westbrook, C. K.; Vincitore, A. M.; Castaldi, M. J.; Senkan, S. M.; Melius, C. F. Aromatic and polycyclic aromatic hydrocarbon formation in a laminar premixed *n*-butane flame. *Combust. Flame* **1998**, *114*, 192−213.

(21) Marinov, N. M.; Pitz, W. J.; Westbrook, C. K.; Castaldi, M. J.; Senkan, S. M. Modeling of aromatic and polycyclic aromatic hydrocarbon formation in premixed methane and ethane flames. *Combust. Sci. Technol.* **1996**, *116*−*117*, 211−287.

(22) Melius, C. F.; Colvin, M. E.; Marinov, N. M.; Pit, W. J.; Senkan, S. M. Reaction mechanisms in aromatic hydrocarbon formation involving the C_5H_5 cyclopentadienyl moiety. *Symp. Int. Combust. Proc.* **1996**, *26*, 685−692.

(23) Zhang, T. C.; Wang, J.; Yuan, T.; Hong, X.; Zhang, L. D.; Qi, F. Pyrolysis of methyl *tert*-butyl ether (MTBE). 1. Experimental study with molecular-beam mass spectrometry and tunable synchrotron VUV photoionization. *J. Phys. Chem. A* **2008**, *112*, 10487−10494.

(24) Zhang, T. C.; Zhang, L. D.; Hong, X.; Zhang, K. W.; Qi, F.; Law, C. K.; Ye, T. H.; Zhao, P. H.; Chen, Y. L. An experimental and theoretical study of toluene pyrolysis with tunable synchrotron VUV photoionization and molecular-beam mass spectrometry. *Combust. Flame* **2009**, *156*, 2071−2083.

(25) Yang, Z.; Zhang, T.; Pan, Y.; Hong, X.; Tang, Z.; Qi, F. Electrospray/VUV single-photon ionization mass spectrometry for the analysis of organic compounds. *J. Am. Soc. Mass Spectrom.* **2009**, *20*, 430−434.

(26) Zhou, Z. Y.; Xie, M. F.; Wang, Z. D.; Qi, F. Determination of absolute photoionization cross-sections of aromatics and aromatic derivatives. *Rapid. Commun. Mass Spectrom.* **2009**, *23*, 3994−4002.

(27) Gans, B.; Garcia, G. A.; Boye-Peronne, S.; Loison, J. C.; Douin, S.; Gaie-Levrel, F.; Gauyacq, D. Absolute photoionization cross section of the ethyl radical in the range 8−11.5 eV: Synchrotron and vacuum ultraviolet laser measurements. *J. Phys. Chem. A* **2011**, *115*, 5387−5396.

(28) National Synchrotron Radiation Laboratory. *Photonionization Cross Section Database*; National Synchrotron Radiation Laboratory: Hefei, China, 2011.

(29) Frisch, M. J.; Trucks, G. W.; Schlegel, H. B.; Scuseria, G. E.; Robb, M. A.; Cheeseman, J. R.; Scalmani, G.; Barone, V.; Mennucci, B.; Petersson, G. A.; Nakatsuji, H.; Caricato, M.; Li, X.; Hratchian, H. P.; Izmaylov, A. F.; Bloino, J.; Zheng, G.; Sonnenberg, J. L.; Hada, M.; Ehara, M.; Toyota, K.; Fukuda, R.; Hasegawa, J.; Ishida, M.; Nakajima, T.; Honda, Y.; Kitao, O.; Nakai, H.; Vreven, T.; Montgomery, J. A., Jr.; Peralta, J. E.; Ogliaro, F.; Bearpark, M.; Heyd, J. J.; Brothers, E.; Kudin, K. N.; Staroverov, V. N.; Kobayashi, R.; Normand, J.; Raghavachari, K.; Rendell, A.; Burant, J. C.; Iyengar, S. S.; Tomasi, J.; Cossi, M.; Rega, N.; Millam, J. M.; Klene, M.; Knox, J. E.; Cross, J. B.; Bakken, V.; Adamo, C.; Jaramillo, J.; Gomperts, R.; Stratmann, R. E.; Yazyev, O.; Austin, A. J.; Cammi, R.; Pomelli, C.; Ochterski, J. W.; Martin, R. L.; Morokuma, K.; Zakrzewski, V. G.; Voth, G. A.; Salvador, P.; Dannenberg, J. J.; Dapprich, S.; Daniels, A. D.; Farkas, O.; Foresman, J. B.; Ortiz, J. V.; Cioslowski, J.; Fox, D. J. *Gaussian 09, Revision A.02*; Gaussian, Inc.: Wallingford CT, 2009.

(30) Schwabe, T.; Grimme, S. Towards chemical accuracy for the thermodynamics of large molecules: New hybrid density functionals including non-local correlation effects. *Phys. Chem. Chem. Phys.* **2006**, *8*, 4398−4401.

(31) Thom, H.; Dunning, J. Gaussian basis sets for use in correlated molecular calculations. I. The atoms boron through neon and hydrogen. *J. Chem. Phys.* **1989**, *90*, 1007−1023.

(32) Kendall, R. A.; Thom, H.; Dunning, J.; Harrison, R. J. Electron affinities of the first-row atoms revisited. Systematic basis sets and wave functions. *J. Chem. Phys.* **1992**, *96*, 6796−6806.
(33) Shi, J.; Huang, X.-Y.; Wang, J.-P.; Li, R. A theoretical study on C−COOH homolytic bond dissociation enthalpies. *J. Phys. Chem. A* **2010**, *114*, 6263−6272.
(34) Erman, P.; Karawajczyk, A.; Rachlewkallne, E.; Stromholm, C.; Larsson, J.; Persson, A.; Zerne, R. Direct determination of the ionization-potential of CO by resonantly enhanced multiphoton ionization mass spectroscopy. *Chem. Phys. Lett.* **1993**, *215*, 173−178.
(35) Moskaleva, V. L.; Madden, K. L.; Lin, C. M. Unimolecular isomerization/decomposition of *ortho*-benzyne: Ab initio MO/statistical theory study. *Phys. Chem. Chem. Phys.* **1999**, *1*, 3967−3972.
(36) Moskaleva, L. V.; Lin, M. C. Unimolecular isomerization/decomposition of cyclopentadienyl and related bimolecular reverse process: Ab initio MO/statistical theory study. *J. Comput. Chem.* **2000**, *21*, 415−425.
(37) Hidaka, Y.; Nakamura, T.; Miyauchi, A.; Shiraishi, T.; Kawano, H. Thermal decomposition of propyne and allene in shock waves. *Int. J. Chem. Kinet.* **1989**, *21*, 643−666.
(38) Miller, J. A.; Melius, C. F. Kinetic and thermodynamic issues in the formation of aromatic compounds in flames of aliphatic fuels. *Combust. Flame* **1992**, *91*, 21−39.
(39) Dagaut, P.; Cathonnet, M. A comparative study of the kinetics of benzene formation from unsaturated C_2 to C_4 hydrocarbons. *Combust. Flame* **1998**, *113*, 620−623.
(40) Scheer, A. M.; Mukarakate, C.; Robichaud, D. J.; Ellison, G. B.; Nimlos, M. R. Radical chemistry in the thermal decomposition of anisole and deuterated anisoles: An investigation of aromatic growth. *J. Phys. Chem. A* **2010**, *114*, 9043−9056.
(41) Lamprecht, A.; Atakan, B.; Kohse-Höinghaus, K. Fuel-rich flame chemistry in low-pressure cyclopentene flames. *Proc. Combust. Inst.* **2000**, *28*, 1817−1824.
(42) Dubnikova, F.; Lifshitz, A. Ring expansion in methylcyclopentadiene radicals. Quantum chemical and kinetics calculations. *J. Phys. Chem. A* **2002**, *106*, 8173−8183.
(43) Lifshitz, A.; Tamburu, C.; Suslensky, A.; Dubnikova, F. Decomposition and ring expansion in methylcyclopentadiene: Single-pulse shock tube and modeling study. *Proc. Combust. Inst.* **2005**, *30*, 1039−1047.
(44) Sharma, S.; Green, W. H. Computed rate coefficients and product yields for *c*-C_5H_5 + CH_3 → products. *J. Phys. Chem. A* **2009**, *113*, 8871−8882.
(45) Yang, J. Z.; Zhao, L.; Cai, J. H.; Qi, F.; Li, Y. Y. Photoionization mass spectrometric and kinetic modeling of low-pressure pyrolysis of benzene. *Chin. J. Chem. Phys.* **2013**, *26*, 245−251.
(46) Gray, P.; Williams, A. Chemistry of free radicals containing oxygen. Part 3. Thermochemistry and reactivity of the higher alkoxyl radicals RO. *Trans. Faraday Soc.* **1959**, *55*, 760−777.
(47) Ruscic, B.; Boggs, J. E.; Burcat, A.; Császár, A. G.; Demaison, J.; Janoschek, R.; Martin, J. M. L.; Morton, M. L.; Rossi, M. J.; Stanton, J. F.; Szalay, P. G.; Westmoreland, P. R.; Zabel, F.; Bérces, T. IUPAC critical evaluation of thermochemical properties of selected radicals. Part I. *J. Phys. Chem. Ref. Data* **2005**, *34*, 573−656.
(48) Blanksby, S. J.; Ellison, G. B. Bond dissociation energies of organic molecules. *Acc. Chem. Res.* **2003**, *36*, 255−263.